Available online at www.sciencedirect.com
SCIENCE DIRECT
Polymer 47 (2006) 2791–2801
polymer
www.elsevier.com/locate/polymer

On the characterization of tensile creep resistance of polyamide 66 nanocomposites. Part I. Experimental results and general discussions

Jing-Lei Yang [a], Zhong Zhang [a,b,*], Alois K. Schlarb [a], Klaus Friedrich [a]

[a] *Institute for Composite Materials, University of Kaiserslautern, 67663 Kaiserslautern, Germany*
[b] *National Center for Nanoscience and Technology, No. 2, 1st North Street Zhongguancun, 100080 Beijing, China*

Received 10 January 2006; received in revised form 19 February 2006; accepted 21 February 2006
Available online 13 March 2006

Abstract

Relatively poor creep resistance is considered as a deficiency of thermoplastics in general. Our previous study [1] on the enhanced creep resistance of polyamide 66 by a very low filler content of spherical nanoparticles explored an exciting phenomenon, which is expected to be able to promote the engineering applications of these materials. In order to comprehensively and deeply understand the effect of nanoparticles, here we provide a systematic investigation on various kinds of nanofillers, i.e. spherical particles and nanoclay, modified polyamide 66 under different stress levels (20, 30 and 40 MPa) at room and elevated temperatures (23, 50 and 80 °C), respectively. Static tensile tests are also performed at corresponding temperatures. Creep was characterized by considering the isochronous stress–strain curves, creep rate, and creep compliance with influence of temperature and stress, respectively. It was found that the creep resistance of nanocomposites was significantly enhanced by nanoparticles without sacrificing the tensile properties. The orientational hardening, as well as the thermal and stress activated process are briefly introduced in order to understand the mechanisms of viscoelasticity of these nanocomposites.

Keywords: Tensile creep; Polymer nanocomposites; Viscoelasticity

1. Introduction

Nanocomposites have been increasingly focused as a novel field in materials science in recent years [2–4]. The mechanical properties of polymer nanocomposites have been extensively studied and many enhanced performances, such as strength, stiffness, toughness, flame retardancy and gas permeability etc., have been achieved to extend the possible applications [5–14]. Some important factors, such as filler concentration, dispersion state and interfacial bonding, are considered to be able to significantly influence the properties of bulk materials. Due to their tiny size and huge interfacial area of nanofillers, a low concentration is usually preferred in most of the current studies. In order to get well-dispersed nanofillers with reduced agglomerates that always impair the performance of composites, surface modifications of nanofillers have been introduced and developed [15–18]. For example both dispersion quality and interfacial bonding could be enhanced by plasma coating in carbon nanofibers reinforced polystyrene [19]. Nevertheless, it is still an exciting topic ongoing with various approaches to improve those two features simultaneously [20]. Recent reports [21–23] on the increase of the glass transition temperature of polymers by the addition of nanoclay or nanoparticles demonstrated that a good bonding between particles and polymer matrix may be expected, thus restricting the mobility of polymer chains. However, it is clear that the potential property improvements on polymer nanocomposites are still not yet fully explored.

Creep is a time-dependent deformation, which takes place under stresses lower than the yielding strength of materials. A recent report [24] showed that nanosized carbonitride dispersions could significantly improve the creep strength of steel at high temperatures. However, relatively poor creep resistance and dimensional stability of thermoplastics are generally a deficiency, impairing the service durability and safety, which is a big barrier for their further expansion of applications, e.g. in automotive and aviation industries. Consequently, studies on creep of these new promising nanocomposites are very important and necessary. Pegoretti et al. [25] observed the creep performance of recycled polyethylene terephthalate (PET) filled with layered silicate. They obtained a slightly decreased creep compliance and

* Corresponding author. Address: National Center for Nanoscience and Technology, No. 2, 1st North Street Zhongguancun, 100080 Beijing, China.
E-mail address: zhong.zhang@nanoctr.cn (Z. Zhang).

0032-3861/$ - see front matter © 2006 Elsevier Ltd. All rights reserved.
doi:10.1016/j.polymer.2006.02.065

no-rising creep rate in composites rather than in neat matrix. More recently, Ranade et al. [26] studied polyethylene/montmorillonite layered silicate (PE/MLS) films and found that the presence of rigid MLS contributed to the improved creep resistance of composites. Vlasveld et al. [27] also studied the effects of physical aging time and moisture on the creep properties of polyamide 6 (PA6) filled by layered silicate. They carried out that the creep compliance of composites could be greatly reduced compared to that of neat PA6. It seems that the current studies on creep performance are mainly focused on layered silicate filled thermoplastic polymers. Moreover, the creep experiments were carried out in a rather short term (the maximum observed time scale among those studies is 1000 min by Ranade et al. [26]). Therefore, long-term influence on creep performance of nanoparticles filled thermoplastics has scarcely been conducted.

Our formerly tentative study carried out the enhanced long-term creep resistance of TiO_2-nanoparticle/polymer nanocomposites [1]. To promote this study, here we performed a systematic research on the creep performances of different fillers with 1 vol% of nanoclay and nanoparticles modified polyamide 66 (PA66) matrix. The experiments were processed under various constant loads (20, 30 and 40 MPa) at room and elevated temperatures (23, 50 and 80 °C), respectively. The influence of different nanofillers on the creep behaviors was investigated, and the creep characterization of nanocomposites was systematically analyzed under diverse testing conditions. Thermally and stress activated process methods were briefly introduced to generally understand the viscoelasticity and creep performances of nanocomposites.

2. Tensile creep of polymers

In general, the originally obtained data are creep strain (ε) and creep time (t), a schematic curve of which is shown in Fig. 1(a) additionally with the calculated creep rate $\dot{\varepsilon}$. According to the curve the entire processes in creep of polymers can be considered as four stages, namely (I) instantaneous deformation with ε_0, (II) primary creep with ε_1, (III) secondary creep with ε_2, and (IV) tertiary creep with ε_3 [28] The instantaneous elongation is due to the elastic or plastic deformation of polymer once the external load is applied, and this stage is independent of time. In the primary creep stage, the creep rate starts at a relatively high value, while decreases rapidly with time, which may be resulted from the slippage and orientation of polymer chains under persistent stress. After a certain period of time, the creep rate reaches a steady-state value in the secondary creep stage, in which the viscoelastic flow in the polymer occurs and the duration is relatively very long if under low stress level. Finally, the material falls into the tertiary creep stage, where the creep rate increases rapidly and final creep rupture or advanced necking occurs, as illustrated in Fig. 1(a).

In addition, creep compliance, $J(t,\sigma(t),T)$, is also frequently applied to describe the creep performance. It can be obtained

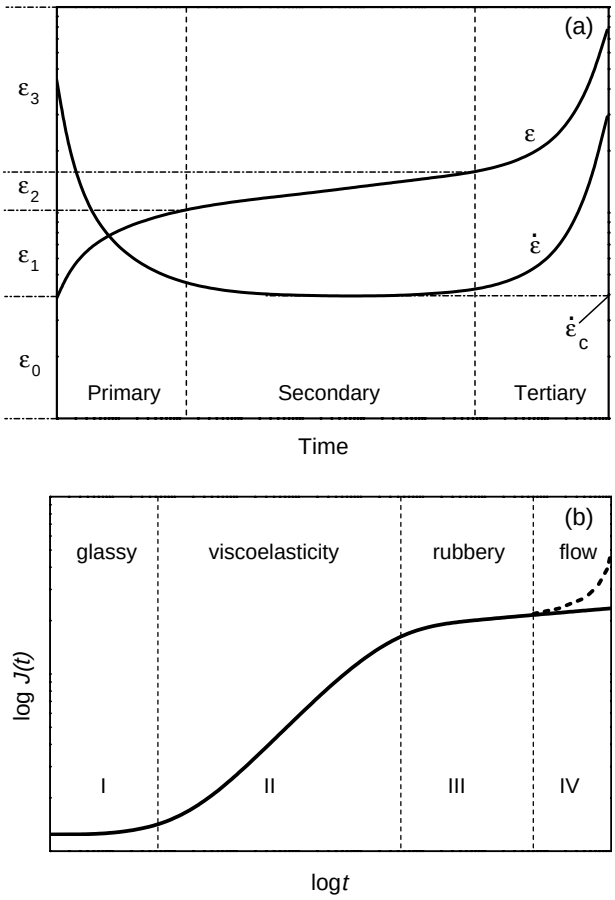

Fig. 1. Schematic creep stages by (a) creep strain and (b) creep compliance.

from the following relation:

$$J(t,\sigma(t),T) = \frac{\varepsilon(t,\sigma(t),T)}{\sigma_0} \tag{1}$$

where t is creep time, $\sigma(t)$ real stress, σ_0 initially applied stress, T temperature, and $\varepsilon(t,\sigma(t),T)$ creep strain dependent on creep time, real stress and temperature. For the case of small deformation, the real stress is normally considered as the same as initial stress and thus the strain is proportional to the initial stress, so we have

$$\varepsilon(t,\sigma(t),T) = \varepsilon(t,\sigma_0,T) = \varepsilon(t,T)c\sigma_0 \tag{2}$$

Therefore, Eq. (1) can be simplified as

$$J(t,\sigma(t),T) = J(t,T) = c\varepsilon(t,T) \tag{3}$$

where c is constant. In Eq. (3), creep compliance is only a function of creep time and temperature applied and, therefore, considered as a material constant for linear solids at constant temperature. A schematic curve of creep compliance vs. time at constant temperature over a very wide time scale is shown in Fig. 1(b). An idealized amorphous polymer will behave as glassy solid, viscoelastic solid, rubber or viscous liquid depending on the time scale or on the temperature of the experiment [29]. The diagram shows that for very short-time experiments the obtained compliance lies at low value in glassy status and is time independent. At enough long time scale, the

polymers become rubbery and present a plateau with time independent. At intermediate time, the compliance lies between these statuses and is time dependent, which is the general situation of viscoelastic behavior. However, at elevated temperatures the polymers will act as viscous flow even though for a short time experiment, which is the basis of time–temperature superposition principle and will be discussed in a followed contribution [30].

3. Experimental

3.1. Materials

A commercial polyamide 66 (PA66, DuPont Zytel 101) was considered as matrix material. Two sizes of TiO_2 particles, with diameters of 300 nm (Kronos 2310) and 21 nm (Aeroxide P25), respectively, were applied as fillers. To improve the dispersion situation of nanoparticles when mixed into the matrix, surface modified 21 nm-TiO_2 particles (Aeroxide T805) were also considered as an additional filler. Nanoclay (Nanofil 919) was selected as well for comparison purposes due to its different structures and features, which was expected to be able to expand the efficiency of this study. The volume content was set as constant of 1% for all nanoparticles (weight fraction given in Table 1). Hereby, five kinds of specimens named as PA66/300 nm-TiO_2 (PA/300), PA66/21 nm-TiO_2 (PA/21), PA66/surface modified 21 nm-TiO_2 (PA/21-SM), PA66/nanoclay (PA/clay), and neat matrix PA66 were used in this study. The detailed information of materials is listed in Table 1.

3.2. Specimens preparation: extrusion and injection molding

Nanocomposites were compounded using a corotating twin-screw-extruder (Berstoff ZE 25A×44D-UTS). The barrel temperatures were set at 55/260/270/280/285/285/285 /285/285 °C, respectively, a screw speed of 150 rpm, and a final extrusion rate of 9 kg/h. PA66 was dried in a vacuum oven at 70 °C for a minimum of 24 h before extrusion. During melt extrusion, ventilation was kept on to remove trapped air in blends. The processing parameters were optimized in order to achieve a fine nanoparticle distribution. In order to precisely control the filler content of nanoparticles, a commercial twin-screw loss-in-weight feeder (K-Tron Soder K-CL-24-KT20) was applied. After cooling by water bath, the extruder blanks was cut as granules with length in a range of 3–5 mm for further injection molding.

The composites were afterwards manufactured using an injection-molding machine (Alburg Allrounder 320S) as dog boned tensile bars $160\times10\times4$ mm^3, according to the standard [31] for tensile and creep tests. For all blends, the injection parameters were maintained constant. The barrel temperature of the injection-molding machine was selected to be 295 °C. The injection pressure was kept constant at 500 bars, the mold temperature was fixed at 70 °C, and a constant injection speed of 80 ccm/s was applied for all specimens.

3.3. Uniaxial tension

A Zwick universal testing machine (Zwick 1485) was applied for uniaxial tensile testing. Both an extensometer and a 250 kN load cell were equipped for measuring the tensile modulus and strength. The injection molded dog-boned tensile specimens were applied. A gauge length of 50 mm was considered. The crosshead speed was kept constant at 2 mm/min for room temperature and 5 mm/min for elevated temperature measurements. An environmental chamber was used for elevated temperature testing. At least four specimens of each composition were tested, and the average values were reported.

Table 1
Characteristics and tensile properties of specimens applied in this study

Specimen code	PA66	PA/300	PA/21-SM	PA/21	PA/clay
Nanofillers	–	300 nm-TiO_2	Surface modified 21 nm-TiO_2	21 nm-TiO_2	100–500 nm×1 nm clay layer
Manufacture code	Zytel 101	Kronos 2310	Aeroxide T805	Aeroxide P25	Nanofil 919
wt% (1 vol%) of filler	0	3.4	3.4	3.4	1.6
Amount of fillers[a]/mm^3	0	7.1×10^8	2.1×10^{12}	2.1×10^{12}	1.1×10^{11}
Young's modulus (GPa)					
23 °C	2.28±0.04	2.65±0.32, +16%	2.27±0.09, −0.4%	2.76±0.11, +21%	2.77±0.16, +22%
50 °C	1.47±0.03	1.69±0.13, +15%	2.02±0.08, +37%	1.82±0.02, +24%	1.81±0.09, +23%
80 °C	0.86±0.07	1.03±0.06, +20%	0.98±0.10, +14%	1.06±0.07, +23%	1.05±0.08, +22%
Tensile strength (MPa)					
23 °C	75.8±0.7	72.5±4.5, −4%	75.6±2.2, −0.3%	71.7±3.8, −5%	73±1.5, −4%
50 °C	57.2±0.7	59.5±0.5, +4%	60.6±0.6, +6%	61.1±0.2, +7%	58.7±0.6, +3%
80 °C	43.3±1.8	44.8±0.6, +3%	46.6±0.6, +8%	47.5±1.4, +10%	44.8±0.5, +3%
Strain at necking (%)					
23 °C	48.8±1.0	27.83±10, −43%	4.39±1.55, −91%	4.66±2.46, −91%	6.94±3.2, −86%
50 °C	82.2±6.4	40.0±5.0, −51%	48.9±5.8, −41%	37.2±2.5, −55%	43.3±4.7, −47%
80 °C	85.0±3.8	54.7±5.8, −36%	41.0±4.9, −52%	39.8±3.9, −53%	60.0±5.0, −29%

The signs of '+' and '−' show the increased or decreased magnitude of nanocomposites compared to that of neat PA66 by percentage, respectively.
[a] The amount of fillers per mm^3 is calculated on the basis of an ideal dispersion of fillers in matrix.

3.4. Uniaxial tensile creep

Uniaxial tensile creep tests were preformed using a Creep Rupture Test Machine with double lever system (Coesfeld GmbH, Model 2002). Ten specimens can be measured simultaneously in an environmental chamber. Before testing, the desired constant load for each measurement unit was calibrated by using a force transducer. Then the samples were fixed into the clamps without loading. For the elevated temperature measurement, the chamber was preheated to the desired value for at least 48 h before specimens were loaded in order to reach a uniform and steady thermal equilibrium. A gauge length of 30 mm was marked on each specimen, and the elongation was monitored by a video camera, which was equipped with a program controlled step motor and connected to a computer image analysis system during the whole period of creep testing. The creep compliance was calculated by the ratio of the measured creep strain to the initial stress. The measurement procedure was performed based on ASTM 2990-01 [28].

4. Results and discussion

4.1. Tensile properties

The tensile experiments were performed at 23, 50 and 80 °C, respectively. The Young's modulus, tensile strength and elongation at necking were listed in Table 1 with relative deviation. The variation in these mechanical parameters of nanocomposites compared to that of neat matrix was also attached behind the obtained values with sign '+' or '−' showing relatively increased or decreased quantity. It can be seen that the modulus of each material was decreased with increasing temperature. In general, the Young's modulus of the composites was slightly higher than that of matrix, showing the reinforcing effect of nanofillers. Among them PA/21 behaved highest modulus at 23 and 80 °C by 21 and 23%, respectively, compared to that of neat PA66. While at 50 °C, PA/21-SM performed highest modulus by 37% compared to the matrix. The UTS of the composites became a bit lower at room temperature while slightly increased by less than 10% at elevated temperatures compared to that of matrix, as shown in Table 1. However, the ductility of the nanocomposites was obviously deteriorated whatever at ambient or elevated temperatures, as listed in Table 1. The total elongations of nanocomposites were decreased by more than 30% at high temperatures while showed brittleness to some degree at ambient temperature. Conclusively, it was clearly shown that the quasi-static mechanical properties of the composites were not seriously deteriorated as a whole by the addition of nanofillers.

4.2. Creep characterization

Our previous experiments [1] showed the creep behaviors of PA and nanoparticle filled composites under as high load as 80% of the static ultra tensile strength (UTS), which presented some interesting results up to creep failure. Hereby in this work, a systematic study on the creep performances of nanocomposites was carried out under moderately low load levels (20, 30 and 40 MPa) at room and elevated temperatures (23, 50 and 80 °C), therefore, nine kinds of testing conditions in total. The primary and secondary creep stages were investigated for a moderate time scale with more than 200 h. The creep deformation, isochronous stress–strain relationship, creep rate and creep compliance of different kinds of nanofillers modified PA66 will be discussed in the following sections.

4.2.1. Creep deformability and isochronous stress–strain relationship

Some representative curves of creep strain versus creep time of the tested specimens under 40 MPa were illustrated in Fig. 2 at (a) 23 °C, (b) 50 °C, and (c) 80 °C, respectively. The creep stages were clearly shown in the figures as instantaneous deformation, primary and unfinished secondary creep processes. The tertiary stage was, however, not observed here because the creep rupture or failure was not considered under the current condition, under which it would take a very long period of time to make the materials failure.

In Fig. 2, it could be observed that the overall deformations of the nanocomposites were noticeably less than that of neat matrix, which showed the creep resistant performance by the presence of nanofillers. Additionally, the deformations of PA/21-SM and PA/clay were very close at 23 °C, as shown in Fig. 2(a), while the creep strains of PA/300 and PA/clay, and PA/21-SM and PA/21 were of the similar level at 50 and 80 °C, as shown in Fig. 2(b) and (c). Generally, among the nanocomposites PA/21 behaved the best non-deformability under each condition.

To get the detailed deformation behaviors of all tested specimens, the isochronous stress–strain curves at 1, 10 and 100 h were obtained from the creep data and thereafter presented in Figs. 3–5 at 23, 50, and 80 °C, respectively. For the 1-h isochronous curves in Fig. 3(a), the creep strains of small nanoparticles and nanoclay filled PA were very close but less than that of neat PA. However, after 10 h and even longer time PA/21-SM and PA/clay behaved similar deformability

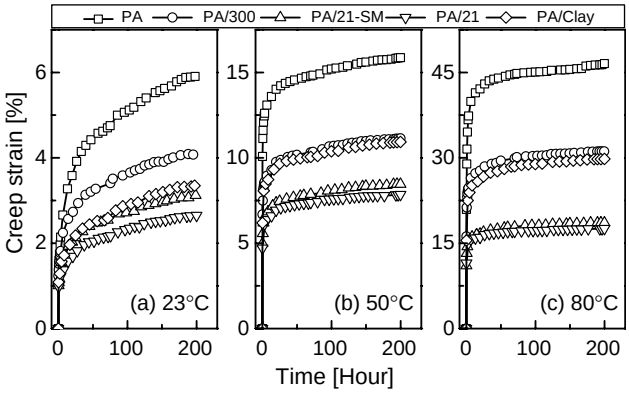

Fig. 2. Curves of creep strain vs. creep time of PA and nanocomposites tested under 40 MPa and (a) 23 °C, (b) 50 °C and (c) 80 °C.

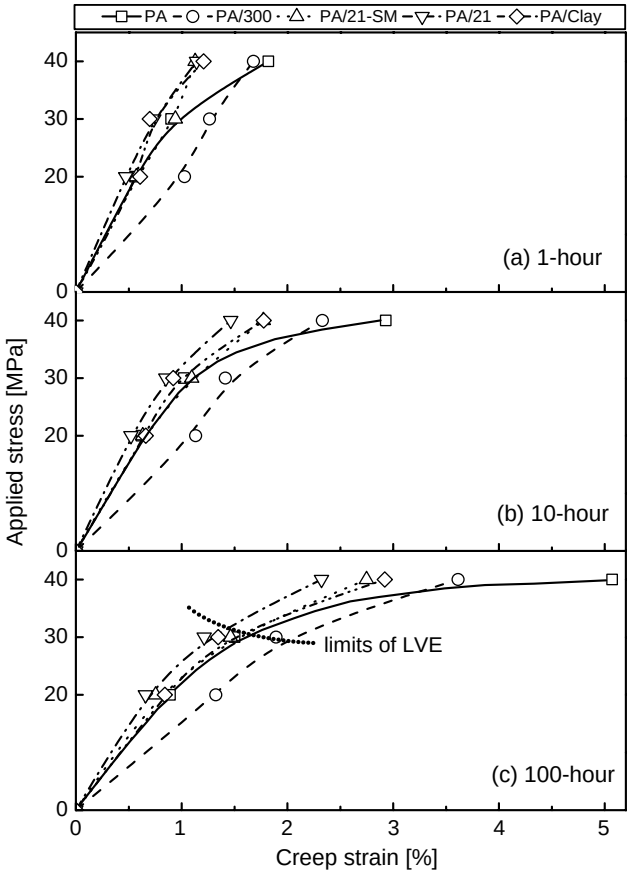

Fig. 3. The isochronous stress–strain relationships of PA and nanocomposites at 23 °C and (a) 1 h, (b) 10 h, and (c) 100 h, respectively.

while PA/21 possessed of the best dimensional stability, as shown in Fig. 3(b) and (c). It was noteworthy to point out that PA/300 exhibited a different isochronous stress–strain relationship with large deformation under the stress not higher than 30 MPa compared to other nanocomposites and neat matrix. The 1-h isochronous strain of the composites showed fairly good linearity with the applied stress even for 40 MPa, under which PA, however, exhibited non-linearity, as shown in Fig. 3(a). This case indicated that the nanofillers extended the linear limits of the matrix within short-time response. With increasing time, the linear relationship between the isochronous stress and strain became worse, particularly under higher stress level, i.e. 40 MPa. However, nanofillers could enhance this linear limit. Among them small nanoparticles were the best, and then nanoclay, while large particles the worst. It could also be found that all of the materials still exhibited linearity under around 30 MPa even at large scale of time, as shown with dot line in Fig. 3(c).

At elevated temperatures, i.e. 50 and 80 °C, the creep deformability of each material became very strong compared to that at 23 °C under the same stress level, as shown in Figs. 4 and 5. Another different scenario from the case at 23 °C was that the deformability of each material at the high temperatures was relatively constant with increasing time after a large instantaneous deformation. This phenomenon indicated there was no pronounced creep deformation in the secondary creep stage, which was also confirmed for example in Fig. 2(b) and (c). It could be clearly discerned there was a three-regime of deformability for the tested specimens: the strongest deformability (PA), the intermediate (PA/300 and PA/clay), and the best non-deformability (PA/21-SM and PA/21). The best reinforcing effectiveness of small particles was again verified. Naturally the non-linearity of the isochronous strain–stress relationship at 80 °C was increased considerably compared to that at 50 °C for each specimen, whereas the linearity was not changed very much with increasing time at constant temperature for each specimen due to the secondary creep deformation insensitive to time, as shown in Figs. 4 and 5. There was also a three-regime of linearity of isochronous stress–strain relationship corresponding to the deformability. The limits of the linearity at 50 °C were higher than that at 80 °C and lower than that at 23 °C for the large scale of time, as marked with dot lines in Figs. 3(c), 4(c) and 5(c). And the limits at 50 °C were in between 20 to 30 MPa with the slight higher values for the nanocomposites, and the same scenario at 80 °C while with the lower limits around 20 MPa.

The materials exhibited different creep deformability and linearity of the isochronous stress–strain relationship at various temperatures and stress levels, which indicated that the filled materials with changed amorphous structures and crystalline morphology had diverse response on temperature, stress level and applied creep time. A representative structure of nanofiller–semicrystalline polymer composites was schematically

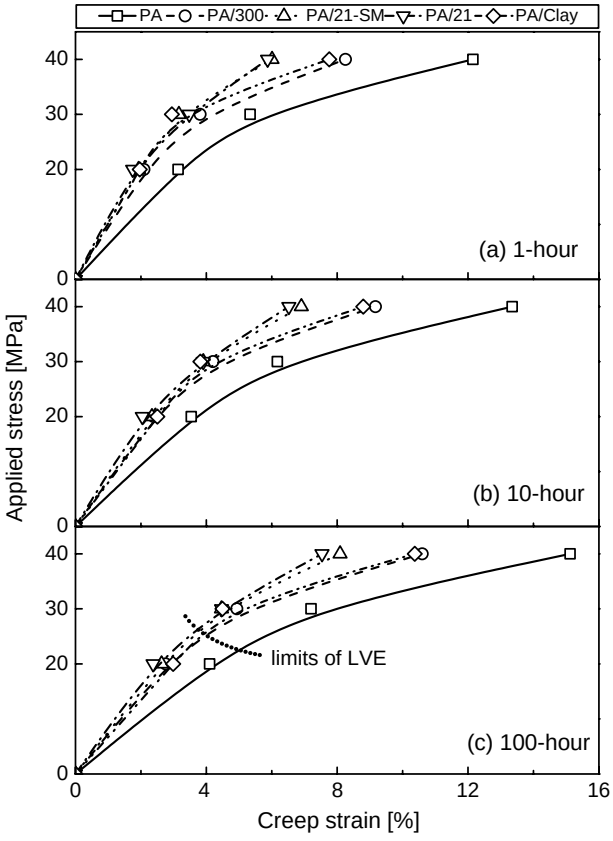

Fig. 4. The isochronous stress–strain relationships of PA and nanocomposites at 50 °C and (a) 1 h, (b) 10 h, and (c) 100 h, respectively.

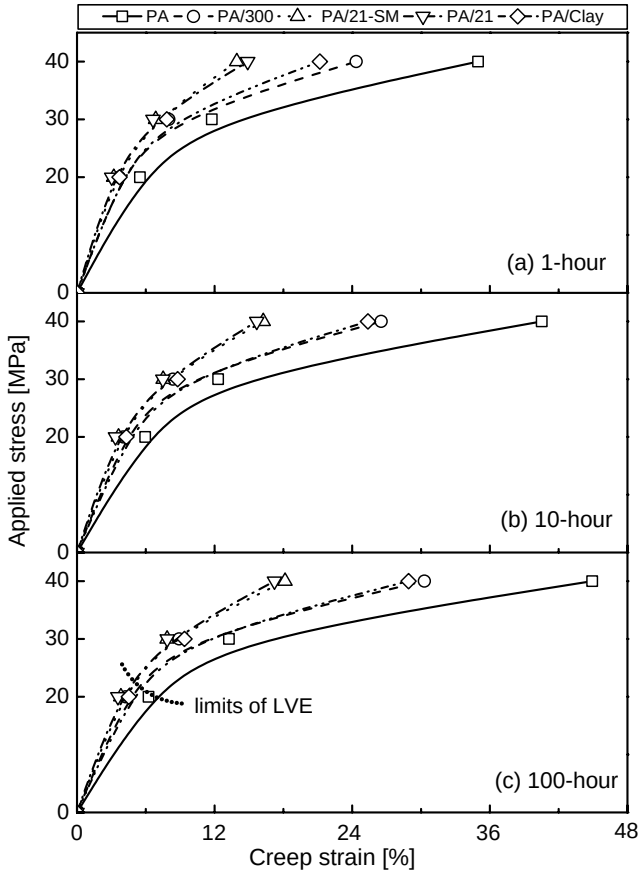

Fig. 5. The isochronous stress–strain relationships of PA and nanocomposites at 80 °C and (a) 1 h, (b) 10 h, and (c) 100 h, respectively.

illustrated in Fig. 6. The essential elements, including crystallized chains, amorphous regions, interphase between filler and matrix, bridging segments between fillers, polymer–filler junction, and dangling end, were considered. The crystallized chains could react rapidly to the external mechanical actions and for example immediately undertake the persistent load [32]. With increasing time, the amorphous regions of the materials were thereafter transferred to bear load, which normally was linear or non-linear viscoelastic processes with orientational

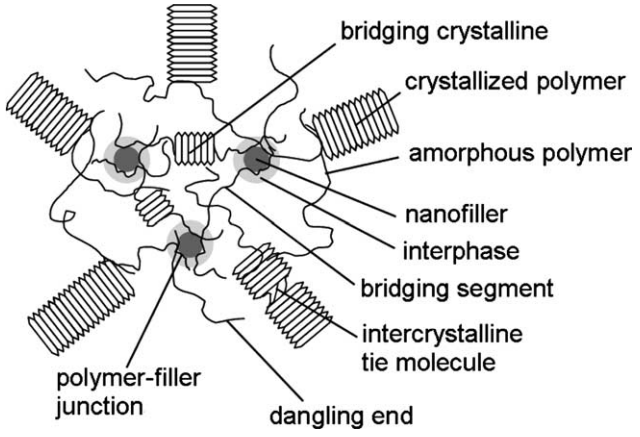

Fig. 6. Schematically representative structure of nanofiller–semicrystalline polymer composites.

strain hardening [33]. In our case of this study the glass transition temperature (T_g) of the nanocomposites was gently increased (less than 4 °C) compared to that of matrix. The crystallinity of the composites was only slightly decreased. However, the crystalline structure and morphology was altered significantly [34] with the micron-sized spherulites in neat matrix instead of sub-micron or nanometric ones. At room temperature, the materials were in glassy state and the mobility of polymer segments was highly restricted. The load bearing ability was very close for the composites due to their similar crystallinity. Additionally the external loads were in the elastic limits of the composites. These might be the reason that all of the composites exhibited a linear relationship between isochronous stress and strain in short response, as shown in Fig. 3(a). With increasing time the rate process in amorphous regions was activated and dominant under high stress level (40 MPa) and resulted in large deformation. From Fig. 3(c) it might also be found a threshold stress around 30 MPa, below which the materials exhibited linearity. The threshold stress of the composites was slightly higher than that of neat PA, as marked by a dot line in the figure.

For comparison, the amount of fillers per cubic millimeter matrix was listed in Table 1 based on the assumption of uniform filler dispersion. Although the agglomerate particles were unavoidable, the huge number of dispersed single particle could form a network [35], which cooperated with the matrix via interphase, bridging segments and junctions to bear load and improve the immobility of polymer chains, as illustrated in Fig. 6. In PA/21 composite, the huge number of fillers (10^{12}mm^{-3}) could form a much dense and stiff network with huge interphase [35]. In this way PA/21 became stiff and resistant to creep deformation. In the case of surface modified nanoparticles although a possible better dispersion could be achieved, the surface strength between particle and matrix, a key factor to affect the reinforcing performance, might be deteriorated due to modification. Considering the as received clay particles with diameter of 35 μm and the individual layer with size of 100–500 nm × 1 nm, it was very difficult to get a full exfoliation into single plates. The shear stress through the interphase could make the non-exfoliated or agglomerate layers to slip [2,36], especially under high stress levels and elevated temperatures. Consequently, PA/clay showed a slightly worse non-deformability and linearity than PA/21. In the case of large particles filled PA, the amount of fillers per cubic millimeter matrix was about 10^9, far less than that of small particles by several orders of magnitude. The size of large particles was in sub-micron level and the defects if any resulted from them were in the same or micron level, which would considerably harm the macro properties of bulk material. Additionally, the network with relatively large interparticle distance was not stiff and weak to restrict the small range of mobility of polymer chains [35], which resulted in worse non-deformability with creep strain $<2\%$ under the stress below 30 MPa compared to that of neat matrix. However, the resistance to deformation of large particles was arose under 40 MPa with strain $>3.5\%$, as shown in Fig. 3(c).

At the point near the glass transition temperature, i.e. 50 °C, polymer chains became active and the mobility of chains was also markedly enhanced due to thermal activation. The deformability thus for example the instantaneous deformation of each material at 50 °C was much severer than that at 23 °C. The deformation after the transient response, however, was insensitive to the rate dependence [37], which was resulted from the rapidly orientational hardening of amorphous regions once the specimen was persistently loaded and the stress was not high enough to produce further deformation of polymer. This was confirmed by the fact that the creep strain of each specimen increased gently and thus the linearity was changed slightly with increasing time from 1 to 100 h, as shown in Fig. 4. In addition, the composites showed fairly good creep resistance compared to neat PA at 50 °C with reduced deformation and enhanced linear viscoelasticity (LVE). The limits of LVE of the tested specimens were in between 20 and 30 MPa, fairly lower than those at 23 °C. The isochronous stress–strain curves in Fig. 4 showed three apparent regimes as mentioned above. The resulting performance of PA/21 very close to that of PA/21-SM indicated the network of particles and interparticle distance rather than interfacial strength played key roles to restrict the mobility of polymer chains. Concerning the interparticle distance, large particles behaved some resistance to relatively large deformation, as mentioned before. In the case of PA/clay, although the interlayer distance might be smaller than that of PA/300, shear stress resulted from large deformation could make slippage in non-exfoliated layers and agglomerate clay particles [2,36], which brought to a worse capability of creep resistance and make PA/clay fall into a similar resulting performance to PA/300, as shown in Fig. 4.

The polymer chains were greatly thermally activated and fairly easy to deform at 80 °C and thus generally the load bearing capability of the bulk specimens became very weak. Consequently, the deformability and linearity of viscoelasticity of the measured specimens at 80 °C were of the similar tendency, however, with much serious extent to those at 50 °C, as shown in Fig. 5. After the severe instantaneous deformation, the creep strain and the non-linear viscoelasticity (NLVE) of each specimen increased weakly from a short time to whatever intermediate or relatively long time scale, as shown in Fig. 5(a)–(c) at 1, 10, and 100 h, respectively. The three similar regimes were still displayed. The limits of the LVE were somehow higher than 20 MPa for composites, however, somewhat lower than 20 MPa for matrix, as approximately indicated in Fig. 5(c) by dot line.

According to the discussion on the isochronous curves, it could be concluded that the deformability and NLVE of each specimen were increased with increasing temperatures and stress levels, and the non-deformability and linearity were enhanced in the hierarchy of (PA66)-(PA/300, PA/clay)-(PA/21-SM, PA/21), where the materials in the same bracket possessed of the close deformation and linearity. Additionally as a quantitative comparison, the material with the maximum decrement in deformation compared to PA66 at the 200th creep hour under each condition was listed in Table 2, almost all of them were PA/21, which exhibited the best performance with most decreased strain by 62% under 80 °C/40 MPa, revealing smaller nanoparticles were the optimum candidate to improve the dimensional stability of bulk material in this study.

Table 2
The nanocomposites with maximum decrement by percentage in creep strain at 200 h and creep rate compared to PA66

	Specimen	Creep strain decrement (%)	Specimen	Creep rate decrement (%)
20 MPa				
23 °C	PA/21	31	PA/21-SM	62
50 °C	PA/21	41	PA/21-SM	46
80 °C	PA/21	43	PA/21	65
30 MPa				
23 °C	PA/21	20	PA/21-SM	31
50 °C	PA/21	38	PA/21	38
80 °C	PA/21-SM	41	PA/21-SM	65
40 MPa				
23 °C	PA/21	55	PA/21	58
50 °C	PA/21	50	PA/21	55
80 °C	PA/21	62	PA/21	67

4.2.2. Creep rate

In addition to deformation, the dimensional stability of materials is determined by another important parameter named creep rate, which represents the velocity of creep deformation. The sample curves of creep rate as a function of time were representatively given in Fig. 7 with PA and PA/21 under different stress levels at 23 °C. In the observed time scope, the creep rate behaved similar trend to creep deformation. In the primary creep stage, the creep rate started at a relatively high value while decreases rapidly with time, which might be due to orientational hardening of materials [38] with instantaneous deformation under sudden and thereafter persistent stress. After a certain period about 50 h, the creep rate entered into a relatively steady status namely as secondary creep stage, in which a dynamic equilibrium of polymer structure evolution and external load was reached. In addition, the creep rate was

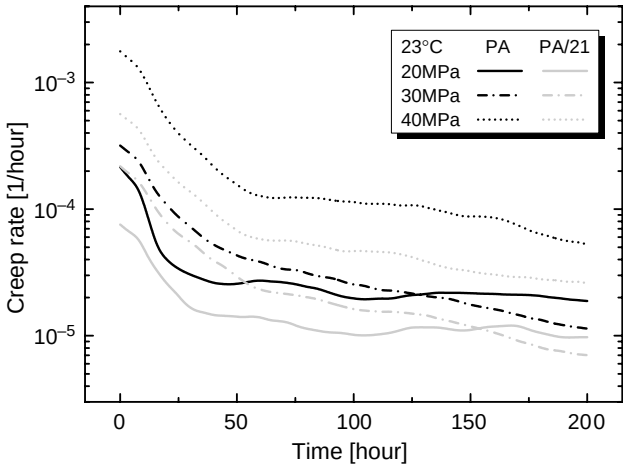

Fig. 7. Sample curves of creep rates of PA and PA/21 as a function of time under different stress levels at 23 °C.

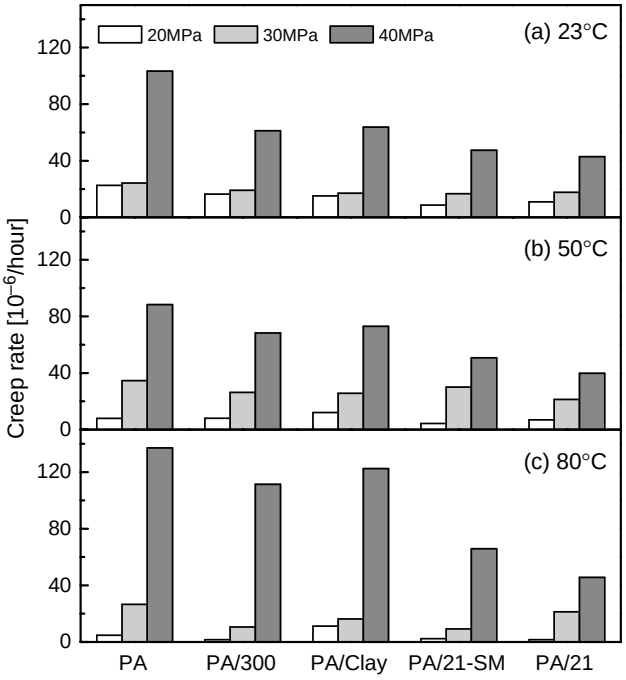

Fig. 8. The influence of stress level on the creep rate of the tested specimens at different temperatures: (a) 23 °C, (b) 50 °C, and (c) 80 °C.

not sensitive to time under 20 MPa while decreased with time under higher stress levels, as shown in Fig. 7. The similar scenarios were also observed at 50 and 80 °C. The creep rate behaved complicated dependence on temperature and stress level compared to deformation and the corresponding discussions were given below.

4.2.2.1. Stress dependence. To simplify, the secondary creep rates of each specimen at different temperatures were then directly fitted and presented as a function of stress level in Fig. 8, from which it could be seen that the materials showed different response to stress levels.

At room temperature, the creep rate of each specimen was insensitive to stress level below 30 MPa while greatly increased under 40 MPa, as shown in Fig. 8(a), which indicated a limit of linear viscoelasticity existed around 30 MPa and the stress activated process was pronounced since the materials behaved non-linear viscoelasticity. At the elevated temperatures, the stiffness of the specimens became weak and the creep rate increased nearly exponentially, especially at 80 °C, as illustrated in Fig. 8(b) and (c). The phenomena implied that the limit of linear viscoelasticity was decreased at elevated temperatures and that the stress activated process became considerable even under intermediate stress levels.

In addition, the creep rates of all nanocomposites were decreased to some extent compared to that of neat PA under each condition. Among them small particles behaved much more effective to decrease creep rate than large ones and clay layers; large nanoparticles and nanoclay layers again behaved close creep rate; surface modification had no positive influence on decreasing creep rate. As analyzed above, the interparticle distance might play a key role to influence the creep rate. For small nanoparticle filled PA, the relatively close interparticle distance and thus a dense particle-network contributed greatly to slow down the deformation speed. However, the large interparticle distance and thus a weak particle-network in large particle and clay layer filled PA were incapable to significantly decrease the creep rate. Moreover, the maximum decrement in creep rate under each condition was listed in Table 2. Among them PA/21 exhibited the lowest value by 67% compared to that of PA66 at 80 °C under 40 MPa, revealing again smaller nanoparticles were the optimum candidate to improve the dimensional stability of bulk material.

4.2.2.2. Temperature effect. The secondary creep rates of each specimen were then redrawn as a function of temperature in Fig. 9 under (a) 20 MPa, (b) 30 MPa, and (c) 40 MPa, respectively. It could be found from the figures that the materials showed much different and complicated dependence on temperature under various stress levels. As discussed above, the specimens behaved linear and non-linear viscoelasticity under the stress levels of 20 and 40 MPa, respectively, within the range of applied temperature; under 30 MPa the materials showed a transition state from linear to non-linear viscoelasticity at the observed temperatures. Hereby we would like to present the discussion by the limits of linearity of viscoelasticity of the samples.

Within the limits of linear viscoelasticity: 20 MPa. The creep rate of each specimen decreased obviously with increasing temperature in the state of linear viscoelasticity, as shown in Fig. 9(a). Under a low stress level of 20 MPa and room temperature, there were no many amounts of polymer segments to be stress activated to involve the creep process in short time. With increasing time, much more segments were

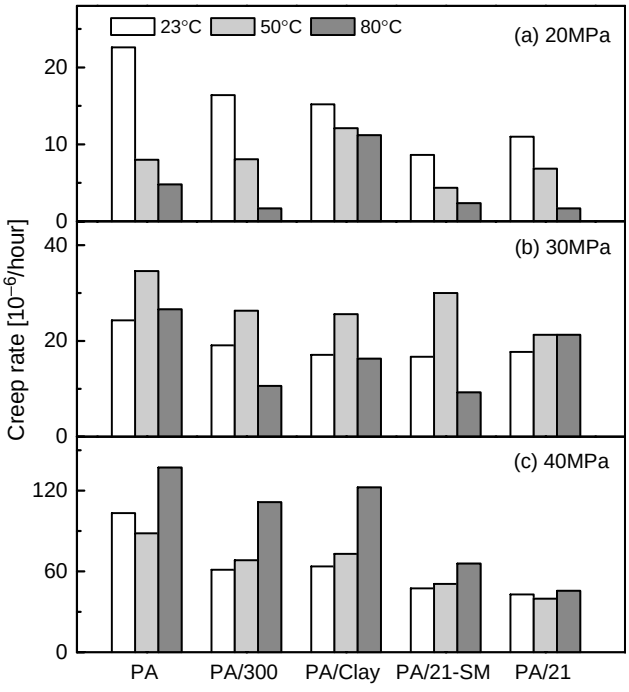

Fig. 9. Comparison of creep rate dependent on temperature for the tested specimens under different stress levels: (a) 20 MPa, (b) 30 MPa, (c) 40 MPa.

activated and brought in relatively high velocity of orientation of polymer segments and entanglements and thus higher creep rate occurred. Although more polymer segments were thermally activated at elevated temperatures than those at RT, the large instantaneous deformation showed that many segments were oriented to some extent along the stress direction in a short time, and thereafter orientational hardening made it much difficult to get further reorientation and rearrangement of polymer chains and entanglements due to relatively small stress level.

In the nanoparticle composites, creep rate decreased with decreasing particle size at the same temperature, showing small particles were more efficient to hinder polymer structure evolution than large sized ones. PA/21-SM possessed lower creep rate at 23 and 50 °C, however, higher rate at 80 °C than PA/21, indicating surface modification worked only under small load level (~0.26 UTS) and below glass temperature while its contribution discounted due to bad interfacial strength at 80 °C. The creep rate of PA/clay was close to that of PA/300 at ambient temperature while much higher than that of PA/300 at 50 and 80 °C, which implied the slippage of non-exfoliated nanoclay layers occurred due to the increasing shear stress caused by serious viscous flow of polymer above glass temperatures.

In the range of non-linear viscoelasticity: 40 MPa. Under 40 MPa creep rate of each specimen generally increased with increasing temperature, as shown in Fig. 9(c). The inverse trend of creep rate in the state of non-linear viscoelasticity indicated the movement of polymer chains was totally different from that in the state of linear viscoelasticity. The creep rate only slightly increased from 23 to 50 °C. This might be due to the serious orientational hardening, which was resulted from thermal activation and high stress level and made it hard to produce advanced speed for the instantaneously oriented polymer chains. However, at 80 °C polymer chains were highly thermally activated and further velocity could be stress activated to overcome the severe orientational hardening.

In the case of nanoparticle composites, creep rate decreased with decreasing particle size at the same temperature, however, much higher than the corresponding value under 20 MPa, showing much more activated polymer chains participated in the creep process. The creep rate of PA/300 was much higher than that of PA/21-SM and PA/21, confirming the above conclusion that smaller particles with close interparticle distance and dense network were more efficient to hinder polymer structure evolution than large sized ones. The contribution to creep rate of surface modified particles with possible bad interfacial strength was not more than that of untreated ones. The creep rate of PA/clay was close to that of PA/300 at all temperatures, which indicated again that the slippage of non-exfoliated nanoclay layers, due to the shear stress caused by serious viscous flow of polymer under high stress level, had fairly adverse effect.

Under transition stress region: 30 MPa. As discussed above, the explicit dependence of creep rate on temperature was provided in the range of linear and non-linear viscoelasticity, respectively. However, in the transition state from linear to non-linear viscoelasticity, an interesting scenario happened that the highest creep rate of each specimen occurred at 50 °C rather than at other temperatures, and the creep rate at RT was close to that at 80 °C. The strong orientational hardening due to instantaneous deformation at 80 °C made it much difficult for further accelerating movement of polymer segments because of moderate stress level, which resulted in the similar creep rate at RT and 80 °C. The orientational hardening at 50 °C was weaker than that at 80 °C, and the accelerating movement of polymer chains was further activated by stress with increasing time, which provided high creep rate under this condition.

In the nanoparticle composites, similar temperature dependence of creep rate was observed compared to that under 20 and 40 MPa. PA/21-SM possessed lower creep rate at 23 and 80 °C, however, higher value at 50 °C than PA/21, indicating surface modification worked badly near the glass temperature, where its contribution discounted because of bad incorporation of interfacial strength. The creep rate of PA/clay was similar to that of PA/300 at ambient and elevated temperatures, which implied the slippage of non-exfoliated nanoclay layers occurred due to the shear stress resulted from the flow of polymer chains.

4.2.3. Creep compliance

The curves of creep compliance vs. creep time of tested specimens were obtained under different load and temperatures, as shown in Fig. 10 with the same axial scale. It was clearly seen from the curves that at RT and 50 °C the creep compliance of each specimen was almost overlapped below the stress level of 30 MPa (except for PA/21 under 50 °C/30 MPa), which implied the limits of linear viscoelasticity existed and were consistent with the above discussion. With increase of load, viscous flow became serious and much complicated by the presence of non-linear viscoelasticity. However, at 80 °C polymer chains became much more thermally active and led to

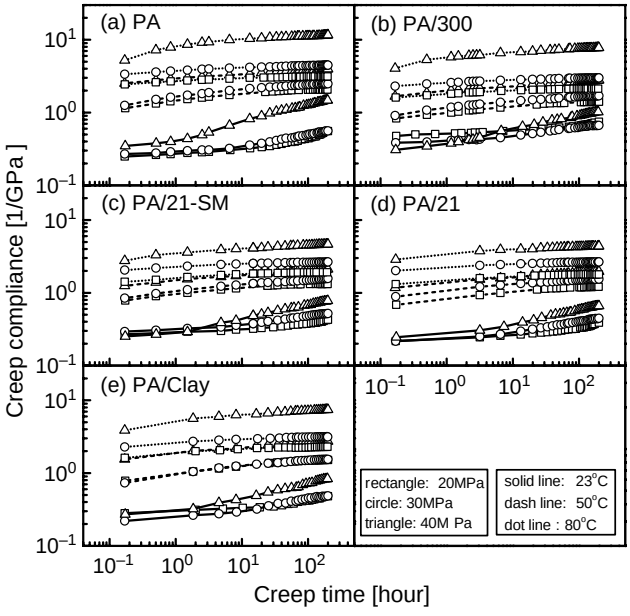

Fig. 10. Stress and temperature dependence of creep compliance of tested specimens: (a) PA, (b) PA/300, (c) PA/21-SM, (d) PA/21, and (e) PA/clay.

apparent non-linear viscoelastic flow even though under as low stress level as 20 MPa. The linearity of viscoelasticity could also be confirmed by the relationship of isochronous stress–strain curves in Figs. 3–5. Another interesting scenario in Fig. 10 was that at 23 °C the tested specimens behaved lower compliance but higher growing rate, however, at temperatures above 50 °C the plateau compliances occurred with much smooth increment, illustrating the materials entered into a rubbery-like or flow state, as demonstrated in Fig. 1(b).

In the case of nanoparticle composites, the compliance was decreased with decreasing particle size at each temperature. At high temperatures, the increment of compliance of small particle filled nanocomposites was much lower than that of large particle filled nanocomposites and matrix. These observed results illustrated that the network formed by small particles was more effective to retard and restrict the movement and evolution of polymer chains than that of large nanoparticles. As for PA/21-SM, its compliance was very similar to that of PA/21 except under the condition of 50 °C/30 MPa, under which PA/21-SM showed better linear property than that of PA/21. This may be due to the well dispersion of surface modified particles contributing more to immobility of polymer chains than untreated particles under that condition. Because of more dispersion of clay layers than that of 300 nm particles in unit volume, the compliance of PA/clay was much lower than that of PA/300 at RT. With increasing temperature serious viscous flow led to high shear stress, which resulted in the slippage of clay layers and discounted the reinforcing effectiveness, and finally the resulting compliance was almost the same as that of PA/300.

5. Conclusions

In the current study, the tensile creep experiments of PA66 and nanocomposites were carried out under different stress levels at room and elevated temperatures. Additionally the static tensile tests were also performed at corresponding temperatures. The creep deformation, isochronous stress–strain relationship, creep rate and creep compliance were obtained and generally discussed by using orientational hardening and thermally and stress activated process methods. Consequently the creep characterization of PA66 and nanocomposites could be concluded as follows:

(1) The static tensile properties of nanocomposites were not seriously deteriorated by the addition of nanofillers compared to those of neat PA66 matrix.
(2) The creep deformation and creep rate behaved complicated dependence on temperature and stress level with thermally and stress activated process. Both the parameters were decreased to different extents by the addition of nanofillers. Amongst them, the most reduction in the creep strain and creep rate was from PA/21 by 62 and 67%, respectively, compared to that of matrix. Accordingly the dimensional stability of the bulk nanocomposites was enhanced.
(3) The limits of linear viscoelasticity could be obtained from the isochronous stress–strain relationship and were decreased with increasing temperature. And the limits of nanocomposites were higher than those of neat matrix, with approximate values of 30 MPa at 23 °C, 20–30 MPa at 50 °C, and 20 MPa at 80 °C, respectively.
(4) The creep compliance confirmed the conclusion obtained in (3). Additionally the creep compliance was decreased by the addition of nanofillers. The rubbery-like or flow state with non-linear viscoelasticity was observed at elevated temperatures.
(5) Finally, the creep resistance was enhanced by the addition of nanofillers. PA/clay exhibited compromised performance close to PA/300 due to the slippage of non-exfoliated clay layers under shear stress resulted from viscous flow of matrix. Although there might be a good dispersion in PA/21-SM, the bad interfacial strength discounted the reinforcing effectiveness under some conditions. When all comes to all, small sized nanoparticle modified PA66 behaved the best creep resistance.

Acknowledgements

Z. Zhang is grateful to the Alexander von Humboldt Foundation for his Sofja Kovalevskaja Award, financed by the German Federal Ministry of Education and Research (BMBF) within the German Government's 'ZIP' program for investment in the future. Additional thanks are due to FACT GmbH for the cooperation of composite injection molding.

References

[1] Zhang Z, Yang J-L, Friedrich K. Creep resistant polymeric nanocomposites. Polymer 2004;45:3481–5.
[2] Pinnavaia TJ, Beall GW. Polymer–clay nanocomposites. New York: Wiley; 2001.
[3] Ajayan PM, Schadler LS, Braun PV. Nanocomposite science and technology. Weinheim: Wiley-VCH; 2003.
[4] Nicolais L, Carotenuto G. Metal–polymer nanocomposites. New York: Wiley; 2005.
[5] Schadler LS, Laul KO, Smith RW, Petrovicova E. Microstructure and mechanical properties of thermally sprayed silica/nylon nanocomposites. J Therm Spray Technol 1997;6:475–85.
[6] Tsai J, Sun CT. Effect of platelet dispersion on the load transfer efficiency in nanoclay composites. J Compos Mater 2004;38:567–79.
[7] Petrovicova E, Knight R, Schadler LS, Twardowski TE. Nylon 11/silica nanocomposite coatings applied by the HVOF process. II. Mechanical and barrier properties. J Appl Polym Sci 2000;78:2272–89.
[8] Kovacevic V, Lucic S, Leskovac M. Morphology and failure in nanocomposites. Part I. Structural and mechanical properties.. J Adhes Sci Technol 2002;16:1343–65.
[9] Garcia M, van Vliet G, Jain S, Schrauwen BAG, Sarkissov A, van Zyl WE, et al. Polypropylene/SiO_2 nanocomposites with improved mechanical properties. Rev Adv Mater Sci 2004;6:169–75.
[10] Krook M, Morgan G, Hedenqvist MS. Barrier and mechanical properties of injection molded montmorillonite/polyesterarnide nanocomposites. Polym Eng Sci 2005;45:135–41.
[11] Phang IY, Liu TX, Mohamed A, Pramoda KP, Chen L, Shen L, et al. Morphology, thermal and mechanical properties of nylon 12/organoclay nanocomposites prepared by melt compounding. Polym Int 2005;54:456–64.

[12] Reddy CS, Das CK. HLDPE/organic functionalized SiO_2 nanocomposites with improved thermal stability and mechanical properties. Compos Interface 2005;11:687–99.
[13] Tjong SC, Bao SP. Impact fracture toughness of polyamide-6/montmorillonite nanocomposites toughened with a maleated styrene/ethylene butylene/styrene elastomer. J Polym Sci, Part B: Polym Phys 2005;43:585–95.
[14] Yang J-L, Zhang Z, Zhang H. The essential work of fracture of polyamide 66 filled with TiO_2 nanoparticles. Compos Sci Technol 2005;65:2374–9.
[15] Kornmann X, Thomann R, Mulhaupt R, Finter J, Berglund L. Synthesis of amine-cured, epoxy-layered silicate nanocomposites: the influence of the silicate surface modification on the properties. J Appl Polym Sci 2002;86:2643–52.
[16] Le Pluart L, Duchet J, Sautereau H, Gerard JF. Surface modifications of montmorillonite for tailored interfaces in nanocomposites. J Adhes 2002;78:645–62.
[17] Tanaka K, Hashimoto K, Kajiyama T, Takahara A. Visualization of active surface molecular motion in polystyrene film by scanning viscoelasticity microscopy. Langmuir 2003;19:6573–5.
[18] Lee SS, Kim J. Surface modification of clay and its effect on the intercalation behavior of the polymer/clay nanocomposites. J Polym Sci, Part B: Polym Phys 2004;42:2367–72.
[19] Shi DL, Lian J, He P, Wang LM, Xiao F, Yang L, et al. Plasma coating of carbon nanofibers for enhanced dispersion and interfacial bonding in polymer composites. Appl Phys Lett 2003;83:5301–3.
[20] Kumar DP, Dadmun MD. Optimization of interfacial interactions to achieve nanoscale dispersion of clay in polymer/clay nanocomposites. Abstr Papers ACS 2004;227:U357.
[21] Potschke P, Fornes TD, Paul DR. Rheological behavior of multiwalled carbon nanotube/polycarbonate composites. Polymer 2002;43:3247–55.
[22] Liu ZJ, Chen KQ, Yan DY. Crystallization, morphology, and dynamic mechanical properties of poly(trimethylene terephthalate)/clay nanocomposites. Eur Polym J 2003;39:2359–66.
[23] Yu ZZ, Yan C, Yang MS, Mai YW. Mechanical and dynamic mechanical properties of nylon 66/montmorillonite nanocomposites fabricated by melt compounding. Polym Int 2004;53:1093–8.
[24] Taneike M, Abe F, Sawada K. Creep-strengthening of steel at high temperatures using nanosized carbonitride dispersions. Nature 2003;424:294–6.
[25] Pegoretti A, Kolarik J, Peroni C, Migliaresi C. Recycled poly(ethylene terephthalate)/layered silicate nanocomposites: morphology and tensile mechanical properties. Polymer 2004;45:2751–9.
[26] Ranade A, Nayak K, Fairbrother D, D'Souza NA. Maleated and non-maleated polyethylene-montmorillonite layered silicate blown films: creep, dispersion and crystallinity. Polymer 2005;46:7323–33.
[27] Vlasveld DPN, Bersee HEN, Picken SJ. The relation between rheological and mechanical properties of PA6 nano and microcomposites. Polymer 2005;46:10279–89.
[28] ASTM D 2990-01. Standard test methods for tensile, compressive, and flexural creep and creep-rupture of plastics. West Conshohocken: ASTM International; 2001.
[29] Ward IM. Mechanical properties of solid polymers. Weinheim: Wiley; 1983.
[30] Yang J-L, Zhang Z, Schlarb A, Friedrich K. On the characterization of tensile creep resistance of polyamide 66 nanocomposites Part II: modeling and prediction of long-term performance. Polymer. Submitted for publication.
[31] DIN EN ISO 527-2. Determination of tensile properties. Part 2. Test conditions for moulding and extrusion plastics. Berlin: Deutsches Insitut fuer Normung; 1996.
[32] van Dommelen JAW, Parks DM, Boyce MC, Brekelmans WAM, Baaijens FPT. Micromechanical modeling of the elasto–viscoplastic behavior of semicrystalline polymers. J Mech Phys Solids 2003;51:519–41.
[33] Harren SV. Toward a new phenomenological flow rule for orientationally hardening glassy-polymers. J Mech Phys Solids 1995;43:1151–73.
[34] Zhang H, Zhang Z, Yang J-L, Friedrich K. Temperature dependence of crack initiation fracture toughness for polyamide nanocomposites. Polymer 2006;47:679–89.
[35] Brechet Y, Cavaille JYY, Chabert E, Chazeau L, Dendievel R, Flandin L, et al. Polymer based nanocomposites: Effect of filler–filler and filler–matrix interactions. Adv Eng Mater 2001;3:571–7.
[36] Aktas L, Hamidi YK, Altan MC. Characterisation of nanoclay dispersion in resin transfer moulded glass/nanoclay/epoxy composites. Plast Rubber Compos 2004;33:267–72.
[37] Sweeney J, Ward IM. A constitutive law for large deformations of polymers at high temperatures. J Mech Phys Solids 1996;44:1033–49.
[38] Harren SV. A yield surface and flow rule for orientationally hardening polymers subjected to arbitrary deformations. J Mech Phys Solids 1997;45:1–20.